An Investigation of the D/H Addition−Elimination and H Atom Abstraction Channels in the Reaction D + H_2CO in the Temperature Range 296 K ≤ *T* ≤ 780 K†

C. Oehlers, H. Gg. Wagner,* and H. Ziemer

Max-Planck-Institut für Strömungsforschung, Bunsenstrasse 10, D-37073 Göttingen, Germany

F. Temps*

Institut für Physikalische Chemie, Universität Kiel, Ohlshausenstrasse 40, D-24098 Kiel, Germany

S. Dóbé

Chemical Research Center, Hungarian Academy of Sciences, Pustaszeri út 59-67, H-1525 Budapest, Hungary

Received: March 31, 2000; In Final Form: July 31, 2000

The reactions of H and D atoms with H_2CO (H + H_2CO → H_2 + HCO (1.1), D + H_2CO → HD + HCO (2.1), and D + H_2CO → H + HDCO (2.2)) have been studied in the temperature range 296 K ≤ *T* ≤ 780 K in an isothermal discharge flow reactor with EPR detection of D and H atoms and LIF detection of HCO. Simultaneous measurements of the absolute concentration−time profiles of the three species established the occurrence of the D/H isotope exchange reaction (2.2) in addition to the H atom abstraction channel (2.1). The rate constants for the three reactions could be represented by the Arrhenius expressions $k_{1.1}(T) = (8.7 \pm 1.9) \times 10^{12} \exp[-(14.5 \pm 0.7)\ \text{kJ mol}^{-1}/RT]\ \text{cm}^3\ \text{mol}^{-1}\ \text{s}^{-1}$, $k_{2.1}(T) = (1.2 \pm 0.5) \times 10^{13} \exp[-(15.8 \pm 0.8)\ \text{kJ mol}^{-1}/RT]\ \text{cm}^3\ \text{mol}^{-1}\ \text{s}^{-1}$, and $k_{2.2}(T) = (5.9 \pm 1.5) \times 10^{12} \exp[-(14.7 \pm 1.0)\ \text{kJ mol}^{-1}/RT]\ \text{cm}^3\ \text{mol}^{-1}\ \text{s}^{-1}$. A mechanistic analysis of reaction 2.2 using the unimolecular rate theory gave these estimates for the classical potential energy barrier heights in the addition of D and H atoms to H_2CO: $\Delta E_0(\text{D} + \text{H}_2\text{CO}) = 1360 \pm 100\ \text{cm}^{-1}$ and $\Delta E_0(\text{H} + \text{H}_2\text{CO}) = 1540 \pm 150\ \text{cm}^{-1}$.

1. Introduction

The chemical and photochemical properties of H_2CO as the prototypical aldehyde molecule have long been of substantial interest.[1−3] In the elementary reactions of H_2CO in the gas phase, the molecule may be attacked by small radicals R in principle either at one of the H atoms or at the CO π bond. The first pathway is expected to lead to HR + HCO via direct H atom abstraction. This reaction is favored because of the relatively weak C−H bond in H_2CO for radicals R which form strong HR bonds. The second pathway is the addition of the attacking radical to the CO moiety, leading to vibrationally excited H_2RCO* and H_2COR* radicals. The subsequent fate of these "chemically activated" species is determined by the competition between unimolecular dissociation and collisional stabilization. However, rather little is known about the addition routes for the different radicals.

In earlier investigations of the elementary reactions of H_2CO with H and O atoms or with OH radicals, the direct H abstraction pathways were usually considered as the important reactions.[4,5] Contributions of the addition channels have occasionally been suggested to explain the observed end product yields, but unambiguous experimental evidence has been lacking. For instance, an addition−elimination channel has been suggested to explain a formation of CO_2 in the reaction O + H_2CO.[6] Results for translationally hot ^{18}O + H_2CO seemed to support the idea of an addition step.[7] However, the existence of an addition channel has been disputed in light of high potential energy barriers calculated for the isomerization and dissociation of the proposed intermediate H_2CO_2* biradical[8] and in light of the results of other experiments complemented with modeling calculations.[9,10] An addition pathway has been verified only for the reaction HO_2 + H_2CO,[11] but this reaction is very slow at room temperature.

This paper reports on a direct investigation of the reaction systems H + H_2CO and D + H_2CO and throws new light on the topic.

The two possible product channels of the H + H_2CO reaction 1 are

$$\text{H} + \text{H}_2\text{CO} \rightarrow \text{H}_2 + \text{HCO} \qquad (1.1)$$

$$\text{H} + \text{H}_2\text{CO} + \text{M} \rightarrow \text{CH}_3\text{O} + \text{M} \qquad (1.2)$$

Reaction 1.1 may be rationalized as a direct H atom transfer step. This reaction is normally assumed as the main channel. CH_3O in reaction 1.2 can be collisionally stabilized only in the high-pressure limit of the reaction.

In contrast, the main reaction pathways of the corresponding D + H_2CO reaction 2 are

$$\text{D} + \text{H}_2\text{CO} \rightarrow \text{HD} + \text{HCO} \qquad (2.1)$$

$$\text{D} + \text{H}_2\text{CO} \rightarrow \text{H} + \text{HDCO} \qquad (2.2)$$

$$\text{D} + \text{H}_2\text{CO} + \text{M} \rightarrow \text{CH}_2\text{DO} + \text{M} \qquad (2.3)$$

Reactions 2.1 and 2.3 are analogous to 1.1 and 1.2. However, different from the situation in the H + H_2CO system where the

† Part of the special issue "C. Bradley Moore Festschrift".

* Corresponding authors. E-Mail for F. Temps: temps@phc.uni-kiel.de.

10.1021/jp0012496 CCC: $19.00
Published on Web 09/23/2000

only dissociation pathway for the intermediate "vibrationally hot" CH_3O^* radical from the addition route leads back to H + H_2CO, the CH_2DO^* complex from the D + H_2CO addition route may also dissociate in the forward direction to give H + HDCO (2.2). The effect of this addition−elimination channel is a D/H isotope exchange. This channel is thermodynamically favored by the change in zero-point energy in HDCO compared to that in H_2CO. Thus, the yields of HD + HCO (2.1) versus H + HDCO (2.2) reflect the branching between the H abstraction and the addition pathways in the system.

Extending some of the initial work at room temperature,[12] we investigated the rate constants and product distributions of reactions 1 and 2 in the temperature range 296 K ≤ T ≤ 780 K at pressures of a few millibars using the discharge flow method with electron paramagnetic resonance (EPR) for the detection of H and D atoms and laser-induced fluorescence (LIF) for the measurement of HCO. The overall rate constants k_1 and k_2 were determined using the pseudo-first-order method with [H_2CO] ≫ [H] and [H_2CO] ≫ [D]. The branching ratios of the two channels of reaction 2 were determined by fitting the rate constants $k_{2.1}$ and $k_{2.2}$ to the measured D, H, and HCO concentration−time profiles. The effects of side and consecutive reactions were taken into account by numerical simulations of the reaction systems and checked by sensitivity analyses. The measured temperature-dependent rate constants encode information on the potential energy barriers in the H + $H_2CO \rightleftarrows CH_3O$ system, which is discussed using transition-state theory.

2. Experimental Section

The reactions were investigated in an isothermal flow reactor consisting of a 100 cm long, 2.2 cm i.d. Suprasil quartz tube equipped with a movable injector connected to the flow tube via stainless steel bellows.[13] The system was thermostated to $\Delta T = \pm 3$ K along the reaction distance ($\Delta z = 50$ cm) using an electrical heating jacket. A calibrated NiCrNi thermocouple inside the injector served for the temperature determination. All glass parts were cleaned with a 5% HF solution and rinsed with distilled water before installation. Room-temperature measurements were made with a thin film of halocarbon wax (Halocarbon Products, 15-00) applied to the reactor walls to reduce heterogeneous reactions; high-temperature experiments were carried out without wall coatings.

The He carrier gas was of the highest commercially available purity (99.9999%; UCAR). H_2 (99.9999%) and D_2 (99.7%) (both Messer Griesheim) were used as supplied or as 1% mixtures with He. All gases passing a microwave discharge were delivered through N_2(l) traps. F_2 (99%, 1% premixed in He; Messer Griesheim) was used for calibrations passed through N_2(l) and NaF traps to remove H_2O and HF traces. NO_2 (≥98%; Messer Griesheim) was used without further purification. H_2CO was generated on-line by the pyrolysis of paraformaldehyde (99%; Fluka) at $T \approx 110$ °C. The glass apparatus for this process was dried at elevated temperature under vacuum prior to use. The paraformaldehyde powder was thoroughly degassed before being heated to remove any air and H_2O. The gaseous H_2CO product was purified by being passed through a series of cold traps at −78 °C before use. All major gas flows were regulated with calibrated mass-flow controllers (Tylan). Trace gases were controlled with needle valves and determined from the pressure rise in calibrated volumes. The pressure in the reactor was measured with a calibrated pressure transducer (MKS) at the lower end of the reaction zone. The usual corrections were applied for viscous pressure drop and back diffusion along the reaction distance.

H, D, and F atoms were generated inside the movable injector by microwave discharge dissociation of the parent molecules diluted in a large excess of He. The F_2 discharge was burning in a quartz tube with a protective alumina tube inside. The dissociation yields were approximately 5−10% for H_2 and D_2 and close to 100% for F_2.

The flow tube was connected to an X-band EPR spectrometer for the H and D atom concentration measurements with a TE_{01n} wide-bore cavity (Varian) located between the pole caps of a 13″ electromagnet (Bruker ER 086C). The field sweep control and the EPR spectrometer were interfaced to a PC microcomputer for signal averaging over a preset number of scans. A cooling jacket (6 cm length) just upstream of the EPR cavity ensured constant detection conditions during the high-temperature measurements. Small amounts of O_2 (10^{-9} mol cm^{-3}) were added through an inlet immediately above the cavity to avoid the saturation of the H and D signals.[14] Numerical simulations showed that this O_2 did not disturb the measurements.

Absolute H and D concentrations were determined using the well-known titration reactions H/D + NO_2. The relative H and D detection sensitivities were checked using the reactions F + $H_2/D_2 \rightarrow$ H/D + HF/DF by the conversion of the F atoms with a large excess of H_2/D_2 and by the theoretical ratio.[14] All three methods agreed to within ±5%. When averaged over 30 scans at a time constant of 0.1 s, the detection limits at a signal-to-noise ratio of 1 were approximately 2×10^9 cm^{-3} for H and 3×10^9 cm^{-3} for D.

HCO radicals were observed by LIF via the $^QR_0(6)$ line of the $\tilde{B}^2A'(0,0,2) \leftarrow \tilde{X}^2A'(0,0,0)$ transition.[15] The detection cell was positioned directly above the EPR cavity for simultaneous measurements with both techniques. The optical specifications were determined by the available narrow space between the coils of the electromagnet. The radicals were excited using a Nd:YAG pump-pulsed dye laser (Quantel International, 661S-20 & Spectra-Physics PDL-3) equipped with a BBO frequency-doubling crystal. The fluorescence was collected at right angles through quartz lenses and a 90° mirror system using a 1″ photomultiplier tube (Thorn-EMI B2F RFI 9235). Suitable filters (Schott UG 11, WG 245) were inserted to reduce scattered laser light. The fluorescence signals were sent to a preamplifier and recorded using a boxcar integrator (Stanford Research SR 250) connected to another PC.

The absolute HCO concentrations were determined by comparing the LIF signals of HCO from the reaction F + H_2CO and the H atom EPR signals from the reaction F + H_2 at fixed initial F atom concentrations. These calibrations were repeated immediately after each experimental run to ensure precise (±10−15%) relative concentration measurements. The detection limit for HCO was ≤2×10^8 cm^{-3}. At the low pressures used, the short radiative lifetime[15] of the $\tilde{B}^2A'(0,0,2)$ state of ∼22 ns eliminated the need to correct for collisional quenching effects. The LIF cell was removed for the overall rate constant measurements.

3. Results

The different elementary reactions in the H + H_2CO and D + H_2CO reaction systems which have to be considered are compiled in Table 1.

The measured concentration−time profiles are governed in the first place by the title reactions 1.1, 2.1, and 2.2.

TABLE 1: Elementary Reactions in the H/D + H_2CO Reaction Systems

reaction	no.	k(296 K), $cm^3\ mol^{-1}\ s^{-1}$	k(600 K), $cm^3\ mol^{-1}\ s^{-1}$	ref
$H + H_2CO \rightarrow H_2 + HCO$	1	2.4×10^{10}	4.8×10^{11}	this work
$D + H_2CO \rightarrow HD + HCO$	2.1	1.9×10^{10}	4.9×10^{11}	this work
$D + H_2CO \rightarrow H + HDCO$	2.2	1.5×10^{10}	3.1×10^{11}	this work
$H + HCO \rightarrow H_2 + CO$	3	7.3×10^{13}	7.3×10^{13}	16
$D + HCO \rightarrow HD + CO$	4.1	6.5×10^{13}	6.5×10^{13}	16
$D + HCO \rightarrow H + DCO$	4.1	1.4×10^{13}	1.4×10^{13}	16
$D + DCO \rightarrow D_2 + CO$	5	7.3×10^{13}	7.3×10^{13}	estmated
$H + DCO \rightarrow HD + CO$	6	7.9×10^{13}	7.9×10^{13}	estimated
$HCO + HCO \rightarrow$ products	7	2.7×10^{13}	2.7×10^{13}	17
$HCO + DCO \rightarrow$ products	8	5.0×10^{13}	5.0×10^{13}	estimated
$DCO + DCO \rightarrow$ products	9	2.7×10^{13}	2.7×10^{13}	estimated
$HCO \rightarrow H + CO$	10	0	2.5×10^{08}	18
$DCO \rightarrow D + CO$	11	0	2.5×10^{08}	estimated
HCO + wall → products	12	20[a]	≤40[a]	this work
DCO + wall → products	13	20[a]	≤40[a]	this work
H + wall → products	14	≤2[a]	≤4[a]	this work
D + wall → products	15	≤2[a]	≤4[a]	this work

[a] First-order rate constant in units of s^{-1}.

TABLE 2: Experimental Results for the Overall Rate Constants for the Reaction H + H_2Co (1)

T, K	p, mbar	v, $m\ s^{-1}$	$[H]_0$, mol cm^{-3}	$[H_2CO]_0$, mol cm^{-3}	k_{1exp}, $[H_2CO]\ s^{-1}$	k_{1exp},[a] $cm^3\ mol^{-1}\ s^{-1}$	k_1,[b] $cm^3\ mol^{-1}\ s^{-1}$
296	1.85	23.8	5.03×10^{-11}	6.19×10^{-10}	24	3.81×10^{10}	3.14×10^{10}
	4.16	10.9	10.9×10^{-11}	9.64×10^{-10}	38	3.93×10^{10}	2.34×10^{10}
	2.14	28.3	3.39×10^{-11}	10.1×10^{-10}	46	4.56×10^{10}	2.13×10^{10}
	3.60	16.7	4.87×10^{-11}	14.5×10^{-10}	74	5.07×10^{10}	2.53×10^{10}
	2.58	32.4	4.80×10^{-11}	15.9×10^{-10}	76	4.79×10^{10}	2.21×10^{10}
	2.97	15.1	4.42×10^{-11}	21.8×10^{-10}	97	4.44×10^{10}	2.20×10^{10}
	2.19	20.8	8.54×10^{-11}	25.8×10^{-10}	112	4.35×10^{10}	2.24×10^{10}
	3.25	18.8	10.3×10^{-11}	31.3×10^{-10}	141	4.50×10^{10}	2.57×10^{10}
402	3.80	19.5	2.68×10^{-11}	3.17×10^{-10}	58	18.2×10^{10}	9.41×10^{10}
	3.54	21.3	2.55×10^{-11}	4.42×10^{-10}	82	18.5×10^{10}	10.1×10^{10}
	2.90	25.8	2.68×10^{-11}	7.95×10^{-10}	154	19.4×10^{10}	9.76×10^{10}
	2.51	29.7	3.43×10^{-11}	8.18×10^{-10}	136	16.7×10^{10}	8.89×10^{10}
	2.49	30.1	3.79×10^{-11}	11.4×10^{-10}	216	19.0×10^{10}	10.5×10^{10}
603	4.06	28.6	1.63×10^{-11}	0.96×10^{-10}	101	$105. \times 10^{10}$	52.6×10^{10}
	5.81	34.7	1.70×10^{-11}	1.08×10^{-10}	91	84.3×10^{10}	43.8×10^{10}
	6.17	40.8	1.26×10^{-11}	1.56×10^{-10}	156	$100. \times 10^{10}$	52.7×10^{10}
	7.01	29.0	1.46×10^{-11}	1.78×10^{-10}	141	79.4×10^{10}	44.3×10^{10}
	6.81	34.4	1.78×10^{-11}	1.83×10^{-10}	146	79.8×10^{10}	47.6×10^{10}
	3.74	30.6	3.62×10^{-11}	2.56×10^{-10}	223	87.3×10^{10}	54.4×10^{10}

[a] Effective overall k_1 value obtained from the measured H atom decay profile. [b] Rate constant value k_1 obtained from the numerical simulation of the reaction system.

Due to the HCO radicals which are formed, additional contributions to the H and D decay arise from the fast radical−radical reactions

$$H + HCO \rightarrow H_2 + CO \quad (3)$$

$$D + HCO \rightarrow HD + CO \quad (4.1)$$

$$D + HCO \rightarrow H + DCO \quad (4.2)$$

The rate constants for both reactions and the product distribution of reaction 4 have been determined previously.[16] Under the conditions, the fast additional H/D atom consumption via reactions 3 and 4 can be accounted for by effective stoichiometry factors n in the experimental H/D decay constants of H_2CO, $n_1 \approx 2$ and $n_2 \approx 1 + k_{2.1}/(k_{2.1} + k_{2.2})$. The reactions

$$H + DCO \rightarrow \text{products} \quad (5)$$

$$D + DCO \rightarrow \text{products} \quad (6)$$

have been included for completeness.

The HCO concentrations are also affected slightly by the mutual combination reactions

$$HCO + HCO \rightarrow \text{products} \quad (7)$$

$$HCO + DCO \rightarrow \text{products} \quad (8)$$

$$DCO + DCO \rightarrow \text{products} \quad (9)$$

and, at high temperature, by the unimolecular dissociation reactions

$$HCO \rightarrow H + CO \quad (10)$$

$$DCO \rightarrow D + CO \quad (11)$$

The additional "wall" reactions of the atoms and radicals (12−15) were measured in the absence of the other reactants. The rate constants are collected in Table 1.

3.1. Rate Constants for the Reaction H + H_2CO. Theoretical measurements for reaction 1 were carried out to obtain a consistent set of data for this system.

3.1.1. Overall Rate Constant Measurements. Reaction 1 was investigated to determine effective overall rate constants at three temperatures in the range 296 K ≤ T ≤ 603 K using the conventional "on/off" pseudo-first-order technique by measuring H atom decay profiles in the presence of a large excess of H_2CO. The experimental conditions and results are compiled in Table 2. The reactant concentrations were varied in the ranges 1×10^{-10} mol $cm^{-3} \leq [H_2CO] \leq 31 \times 10^{-10}$ mol cm^{-3} and 1.2×10^{-11} mol $cm^{-3} \leq [H]_0 \leq 10.9 \times 10^{-11}$ mol cm^{-3}, corresponding to a ratio of $6 \leq [H_2CO]/[H]_0 \leq 50$. H atom decay profiles were monitored for a change of up to 1 order of magnitude in concentration. The measured depletion could be described by the standard rate law as $d\ \ln([H]_{+H_2CO}/[H]_{-H_2CO})/dt = -k_{1exp}[H_2CO]$. With error limits of 2σ, the experimental

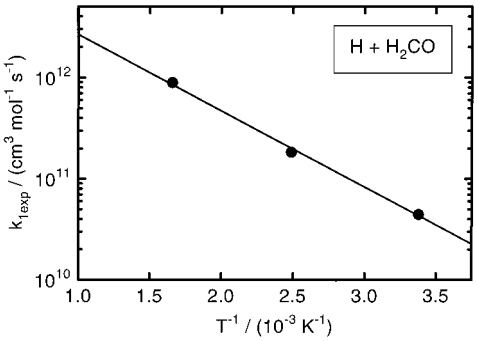

Figure 1. Arrhenius plot of the experimental rate constants k_{1exp} for the reaction H + H_2CO.

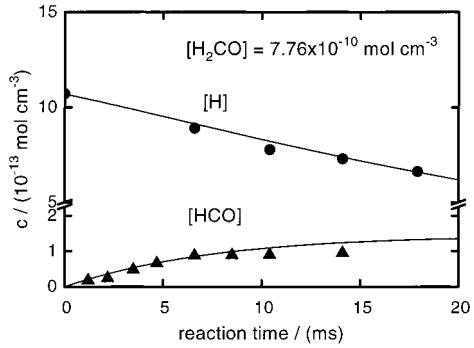

Figure 2. Concentration−time profiles of the H atoms and HCO radicals in the reaction system H + H_2CO (T = 296 K). Measured concentrations: ● = H, ▲ = HCO. Fitted concentration profiles: —.

second-order rate constants k_{1exp} (before correction by the stoichiometry factor) were found to be described by the expression

$$k_{1exp}(T) = (1.5 \pm 0.3) \times 10^{13} \times \exp[-(14.4 \pm 0.6)\ \text{kJ mol}^{-1}/RT]\ \text{cm}^3\ \text{mol}^{-1}\ \text{s}^{-1}$$

An Arrhenius plot of the data is shown in Figure 1.

A detailed analysis of the experiments was performed by numerical simulations of the reaction system (Table 1). The rate constant values for reaction 1 were directly fitted to the experimental H atom profiles by using a program suite based on the Gear algorithm[19] for solving the coupled differential rate equations and the Levenberg−Marquardt nonlinear least-squares fitting algorithm.[20] From these simulations, an effective stoichiometry factor was derived of $n_1 \approx 1.85 \pm 0.05$, depending only slightly on the initial conditions used and close to the value of $n_1 = 2$ assumed above. The final derived Arrhenius expression for $k_1(T)$ in the range 296 K ≤ T ≤ 603 K is

$$k_1(T) = (8.7 \pm 1.9) \times 10^{12} \times \exp[-(14.5 \pm 0.7)\ \text{kJ mol}^{-1}/RT]\ \text{cm}^3\ \text{mol}^{-1}\ \text{s}^{-1}$$

Including possible systematic errors, the uncertainty limits are estimated to be ±20%.

3.1.2. Product Measurements. Additional work was carried out to detect the formation of the HCO radicals. Since HCO and H_2 were the only possible product species under the experimental conditions, these measurements were made only at room temperature. The observed H and HCO concentration−time profiles from one experimental run are shown in Figure 2.

The product measurements were analyzed using the aforementioned program suite by least-squares-fitting the values of k_1 simultaneously to the measured HCO and H profiles. The

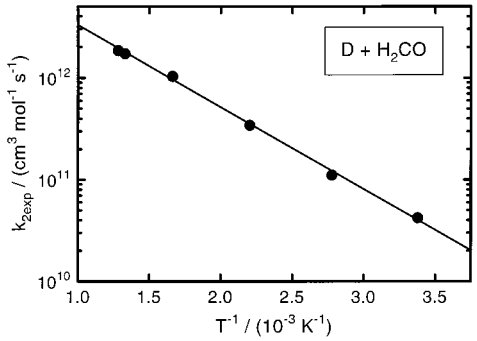

Figure 3. Arrhenius plot of the experimental rate constants k_{2exp} for the reaction D + H_2CO.

statistical weight factors of 0.1 and 1.0 were assigned to the H and HCO concentrations, respectively, in the χ^2 figure-of-merit function in the fitting routine to account for the different magnitudes of the concentrations. The resulting best-fit value for k_1 was

$$k_1(296\ \text{K}) = (2.4 \pm 0.5) \times 10^{10}\ \text{cm}^3\ \text{mol}^{-1}\ \text{s}^{-1}$$

in excellent agreement with the value obtained from the above expression of the H atom decay measurement $k_1(296\ \text{K}) = (2.3 \pm 0.4) \times 10^{10}$ cm^3 mol^{-1} s^{-1}.

3.2. Rate Constants and Product Distribution for the Reaction D + H_2CO. *3.2.1. Overall Rate Constant Measurements.* Reaction 2 was investigated under conditions similar to reaction 1 to determine effective overall rate constant values by monitoring the D atom decay profiles in the presence and absence of a large excess of H_2CO. The conditions and results are summarized in Table 3. Data were collected at six temperatures in the range 296 K ≤ T ≤ 780 K. The reactant concentrations varied in the ranges 0.94×10^{-10} mol cm^{-3} ≤ [H_2CO] ≤ 20×10^{-10} mol cm^{-3} and 0.5×10^{-11} mol cm^{-3} ≤ [D] ≤ 16×10^{-11} mol cm^{-3}, with an excess ratio for most measurements in the range 5 ≤ [H_2CO]/[D]$_0$ ≤ 22. An Arrhenius plot is depicted in Figure 3.

The experimental rate constants could be described by the expression

$$k_{2eff}(T) = (2.1 \pm 0.3) \times 10^{13} \times \exp[-(15.4 \pm 0.4)\ \text{kJ mol}^{-1}/RT]\ \text{cm}^3\ \text{mol}^{-1}\ \text{s}^{-1}$$

The effective stoichiometry factor contained in the expression for $k_{2eff}(T)$ under these conditions is $n_2 \approx 1 + k_{2.1}/(k_{2.1} + k_{2.2})$, depending on the initial [H_2CO]/[D] concentration ratio. A detailed evaluation of the overall rate data was therefore performed iteratively with the analysis of the product measurements.

3.2.2. Product Measurements. Product investigations for reaction 2 were performed at T = 296 and 600 K. The contributions of the H abstraction (2.1) and addition−elimination (2.2) routes were determined by monitoring the formation of the HCO radicals (at 296 K) from reaction 2.1 simultaneously with the D atom decay profiles and, in particular, by monitoring the formation of the H atoms (at 296 and 600 K) from reaction 2.2. The experimental conditions and results are collected in Table 4.

The measurements were made using low initial H_2CO concentrations to resolve the initial rise of the products (4×10^{-10} mol cm^{-3} ≤ [H_2CO]$_0$ ≤ 9×10^{-10} mol cm^{-3} at T = 296 K and 0.6×10^{-10} mol cm^{-3} ≤ [H_2CO]$_0$ ≤ 1×10^{-10} mol cm^{-3} at T = 600 K). Low D atom concentrations were employed

TABLE 3: Experimental Conditions for the Reaction D + H_2CO (2) for Six Temperatures

T, K	p, mbar	v, m s^{-1}	$[D]_0$, mol cm^{-3}	$[H_2CO]_0$, mol cm^{-3}	k_{2exp}, $[H_2CO]$ s^{-1}	k_{2exp},[a] cm^3 mol^{-1} s^{-1}
296	2.25	23.7	15.3×10^{-11}	5.46×10^{-10}	24	4.47×10^{10}
	3.54	15.0	15.3×10^{-11}	5.98×10^{-10}	25	4.10×10^{10}
	3.14	17.0	15.8×10^{-11}	9.43×10^{-10}	41	4.36×10^{10}
	2.75	18.5	12.6×10^{-11}	14.0×10^{-10}	54	3.86×10^{10}
	3.54	15.1	16.1×10^{-11}	14.8×10^{-10}	61	4.10×10^{10}
	2.25	24.1	14.3×10^{-11}	19.1×10^{-10}	86	4.50×10^{10}
	3.75	10.8	16.1×10^{-11}	20.2×10^{-10}	83	4.11×10^{10}
360	2.77	20.2	3.82×10^{-11}	4.36×10^{-10}	42	9.54×10^{10}
	2.65	27.2	3.63×10^{-11}	5.22×10^{-10}	54	10.3×10^{10}
	2.77	22.0	10.1×10^{-11}	7.81×10^{-10}	90	11.5×10^{10}
	3.22	22.4	3.52×10^{-11}	8.69×10^{-10}	105	12.1×10^{10}
	2.37	23.9	3.89×10^{-11}	11.5×10^{-10}	137	11.9×10^{10}
	3.15	19.4	10.3×10^{-11}	14.2×10^{-10}	161	11.3×10^{10}
454	2.63	23.5	3.52×10^{-11}	2.66×10^{-10}	89	33.4×10^{10}
	2.45	27.9	3.35×10^{-11}	4.51×10^{-10}	159	35.4×10^{10}
	2.77	24.7	4.62×10^{-11}	4.64×10^{-10}	159	34.2×10^{10}
	3.26	23.8	3.19×10^{-11}	6.68×10^{-10}	224	33.6×10^{10}
	3.00	22.9	4.10×10^{-11}	8.00×10^{-10}	283	35.3×10^{10}
601	3.87	25.5	2.03×10^{-11}	1.20×10^{-10}	115	95.8×10^{10}
	3.78	27.1	1.93×10^{-11}	1.40×10^{-10}	145	104×10^{10}
	4.08	24.2	1.57×10^{-11}	2.01×10^{-10}	211	105×10^{10}
	3.64	27.2	1.43×10^{-11}	2.67×10^{-10}	294	110×10^{10}
	3.30	31.1	1.84×10^{-11}	2.94×10^{-10}	323	110×10^{10}
	3.42	26.8	1.74×10^{-11}	3.68×10^{-10}	356	96.8×10^{10}
752	4.38	27.5	0.48×10^{-11}	1.10×10^{-10}	190	173×10^{10}
	4.03	29.8	0.96×10^{-11}	1.87×10^{-10}	321	172×10^{10}
780	3.99	28.9	3.04×10^{-11}	0.94×10^{-10}	176	187×10^{10}
	4.66	25.1	1.32×10^{-11}	1.47×10^{-10}	268	182×10^{10}

[a] Effective overall k_2 value obtained from the measured D atom decay profile.

TABLE 4: Experimental Results of the Product Investigation of the D + H_2CO Reaction

T, K	p, mbar	v, m s^{-1}	[D], mol cm^{-3}	$[H_2CO]$, mol cm^{-3}	$k[H_2CO]$, s^{-1}	$k_{2.1}$,[a] cm^3 mol^{-1} s^{-1}	$k_{2.2}$,[a] cm^3 mol^{-1} s^{-1}
296	2.62	17.3	0.80×10^{-12}	4.73×10^{-10}	19	2.05×10^{10}	1.68×10^{10}
	3.50	23.2	1.14×10^{-12}	6.55×10^{-10}	28	1.62×10^{10}	1.38×10^{10}
	3.07	26.9	1.29×10^{-12}	6.91×10^{-10}	32	1.80×10^{10}	1.54×10^{10}
	2.57	29.1	1.49×10^{-12}	7.46×10^{-10}	36	1.88×10^{10}	1.77×10^{10}
	2.00	24.9	2.92×10^{-12}	8.46×10^{-10}	35	1.98×10^{10}	1.54×10^{10}
	2.39	22.5	1.81×10^{-12}	8.68×10^{-10}	35	2.35×10^{10}	1.35×10^{10}
600	4.79	37.7	2.34×10^{-12}	5.77×10^{-11}	58	41.1×10^{10}	33.7×10^{10}
	4.24	38.3	0.92×10^{-12}	5.99×10^{-11}	59	50.5×10^{10}	32.3×10^{10}
	3.90	36.8	1.24×10^{-12}	7.58×10^{-11}	71	50.2×10^{10}	27.9×10^{10}
	3.78	43.1	0.72×10^{-12}	8.00×10^{-11}	82	57.5×10^{10}	33.3×10^{10}
	3.54	40.0	1.38×10^{-12}	8.61×10^{-11}	88	49.8×10^{10}	33.4×10^{10}
	5.29	34.0	1.47×10^{-12}	10.1×10^{-11}	99	45.5×10^{10}	28.2×10^{10}

[a] Values for $k_{2.1}$ and $k_{2.2}$ obtained by least-squares-fitting the numerically simulated concentration profiles simultaneously to the experimental D, H, and HCO profiles.

to reduce the effect of secondary reactions (0.8×10^{-12} mol $cm^{-3} \leq [D]_0 \leq 2.9 \times 10^{-12}$ mol cm^{-3}). Simulations showed that in the first 10−20 ms of the reaction under these conditions the system is governed by reaction 2 and that secondary reactions of the products H and HCO do not play very important roles.

The measured concentration−time profiles at the two temperatures are shown in Figures 4 and 5, respectively. From the observed profiles, it is seen that both HCO and H are formed as primary products of reaction 2 without induction times. At short reaction times, the concentrations of both species are roughly equal, indicating comparable contributions from reactions 2.1 and 2.2. At 296 K, the product concentrations reach their maxima at reaction times longer than the observation times. At 600 K, the H maxima are reached somewhat sooner because of the faster rate of reaction 2. Under all conditions, the H and HCO decay reactions seem to be relatively slow.

Using the numerical simulation-least-squares fitting procedure (reactions in Table 1), the values of the rate constants $k_{2.1}$ and $k_{2.2}$ could be determined by simultaneously fitting them to the measured D, H, and HCO profiles (at 296 K) and the measured D and H profiles (at 600 K). Small adjustments ($\Delta t \leq 1$ ms) of the absolute reaction times were applied to allow for the finite mixing times of the reactants in the flow tube, determined from the intersections of the straight lines in plots of $\ln[D]_{+H_2CO}$ and $\ln[D]_{-H_2CO}$ versus t. The statistical weights of the data for the fitting were 0.1 for D and 1.0 for H and HCO.

The results are given in Table 4. The average values for the rate constants (with 2σ limits) are

$$k_{2.1}(296\ \mathrm{K}) = (1.9 \pm 0.5) \times 10^{10}\ \mathrm{cm^3\,mol^{-1}\,s^{-1}}$$

$$k_{2.2}(296\ \mathrm{K}) = (1.5 \pm 0.4) \times 10^{10}\ \mathrm{cm^3\,mol^{-1}\,s^{-1}}$$

$$k_{2.1}(600\ \mathrm{K}) = (4.9 \pm 0.9) \times 10^{11}\ \mathrm{cm^3\,mol^{-1}\,s^{-1}}$$

$$k_{2.2}(600\ \mathrm{K}) = (3.1 \pm 0.3) \times 10^{11}\ \mathrm{cm^3\,mol^{-1}\,s^{-1}}$$

Thus, the addition−elimination route accounts for approximately 40% of the D + H_2CO reaction. The fitted concentrations can be seen in Figures 4 and 5. The calculated and experimental profiles are in excellent agreement.

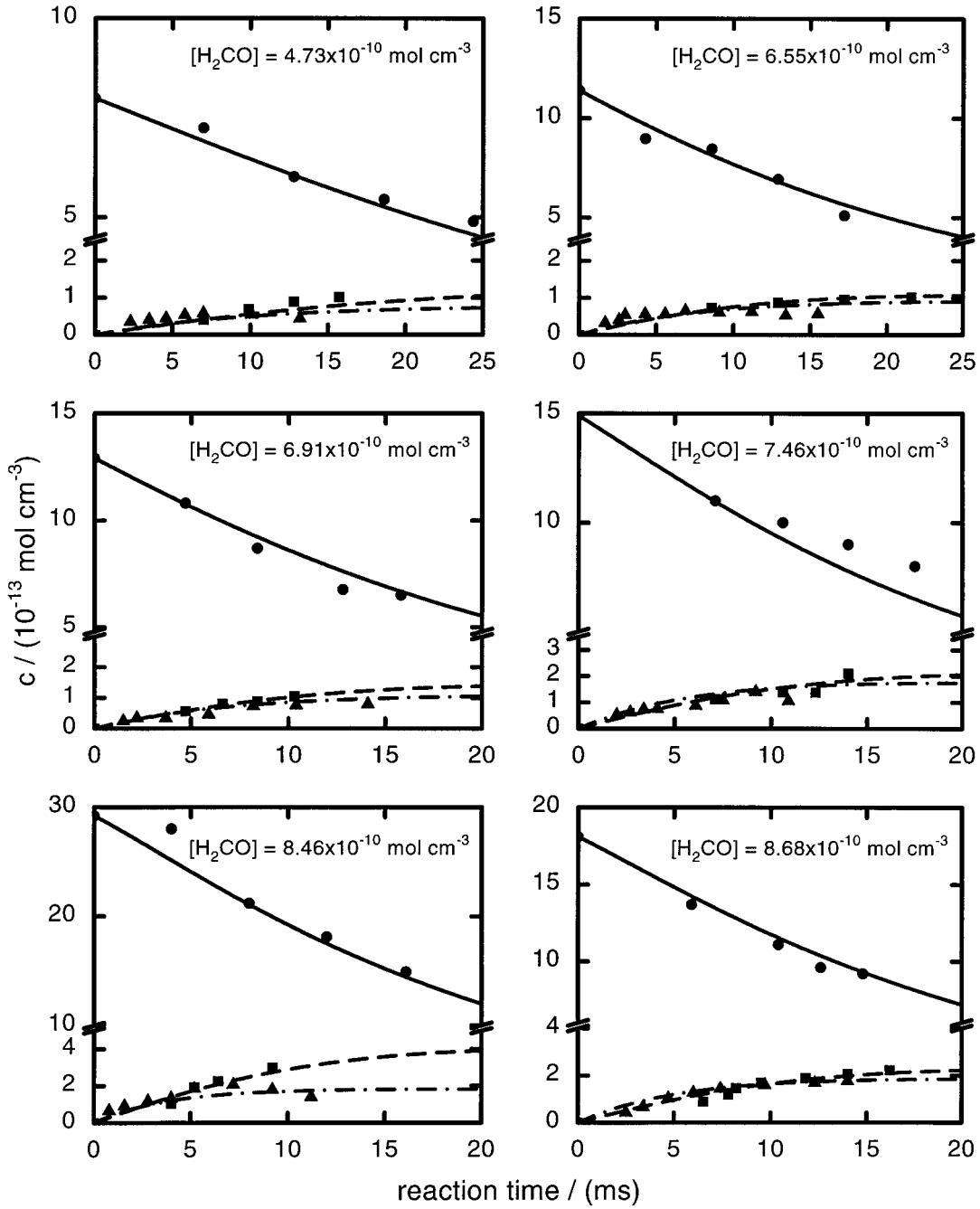

Figure 4. Measured concentration−time profiles of the D and H atoms and HCO radicals in the reaction system D + H_2CO at $T = 296$ K. Experimental concentrations: ● = D, ■ = H, and ▲ = HCO. Fitted concentration profiles: —. The rate constant values $k_{2.1}$ and $k_{2.2}$ from the fitting are given in Table 4.

The results at the two temperatures translate to the respective Arrhenius expressions of

$$k_{2.1}(T) = (1.2 \pm 0.5) \times 10^{13} \times \exp[-(15.8 \pm 0.8)\ \text{kJ mol}^{-1}/RT]\ \text{cm}^3\,\text{mol}^{-1}\,\text{s}^{-1}$$

$$k_{2.2}(T) = (5.9 \pm 1.5) \times 10^{12} \times \exp[-(14.7 \pm 1.0)\ \text{kJ mol}^{-1}/RT]\ \text{cm}^3\,\text{mol}^{-1}\,\text{s}^{-1}$$

with estimated error limits including the systematic errors of the rate constants to within 25%.

3.2.3. Sensitivity Analysis. The influence of the various side reactions on the experimental results at the two temperatures was checked by sensitivity analyses. Histograms of the computed reduced sensitivity coefficients $\delta(\ln c_i)/\delta(\ln k_j)$ for the measured species (D, H, HCO) at $T = 296$ and 600 K can be found in panels a and b, respectively, of Figure 6. The sensitivity coefficients are given at an intermediate reaction time of $\Delta t =$ 10 ms. The influence of the possible secondary reactions, especially the wall loss of the products and their mutual combination reactions, increases with increasing reaction time. Also, the effects are generally somewhat larger at the higher temperature; Figure 6b gives almost the worst case scenario. However, the diagrams show that the concentration profiles are most strongly determined by the values of $k_{2.1}$ and $k_{2.2}$.

4. Discussion

Reaction 1 has previously been studied in a number of laboratories (see refs 4 and 5). The different measurements have been evaluated in some detail by Irdam et al.,[21] who modeled

TABLE 5: Molecular Parameters of the CH_2DO, $H-HDCO^{\ddagger}$, and $D-H_2CO^{\ddagger}$ Used For the Unimolecular Rate Calculations (values in cm^{-1})

	CH_3O[a]	$H-CH_2O^{\ddagger}$[b]	$H + H_2CO$[c]	CH_2DO[d]	$D-CH_2O^{\ddagger}$[d]	$H-CHDO^{\ddagger}$[d]	$D + H_2CO$[c]	$H + HDCO$[c]
ΔH_0^0	−6920	+1540	0	−7470	+1360	+960	0	−590
A	5.210	3.925	9.405	3.910	2.710	3.280	9.405	6.148
B	0.932	1.007	1.295	0.838	0.929	0.905	1.295	1.027
C	0.932	0.962	1.134	0.797	0.808	0.881	1.134	0.894
ν_i	2800	2798	2811	2840	2800	2800	2811	2844
	1359	1593	1500	1360	1590	1450	1500	1400
	1437	1173	1170	1430	1170	1075	1170	1060
	1045	1414	1756	1040	1410	1410	1756	1723
	1038	581	-	900	500	580	-	-
	2809	2892	2861	2800	2890	2150	2861	2121
	1437	740	-	1090	600	650	-	-
	1038	1232	1251	900	1100	1150	1251	1030
	2809	830*i*	-	2300	740*i*	900*i*	-	-
σ	3	1	2	1	1	1	2	1
g_L	2	1	1	2	1	1	1	1
g_S	2	2	2	2	2	2	2	2

[a] Ref 29. [b] Scaled values according to ref 27. [c] Ref 28. [d] This work (estimated).

the rate constant for the $H + H_2CO$ abstraction reaction in a wide temperature range using transition-state theory. The present result for the rate constant $k_1(T)$ fits well with the available body of data. It is important that the results for k_1 from the measurements of the H atom decay and the HCO production at room temperature were found to be in excellent agreement.

The overall rate constant for reaction 2 is somewhat higher than for reaction 1 in the temperature range investigated. The room-temperature value is $k_2(296\ K) = 3.4 \times 10^{10}\ cm^3\ mol^{-1}\ s^{-1}$ compared to $k_1(296\ K) = 2.3 \times 10^{10}\ cm^3\ mol^{-1}\ s^{-1}$. This difference is explained for the most part by the additional contribution from the D/H isotope exchange process (2.2), which accounts for ~40% of the overall reaction. On the other hand, the H atom abstraction channel is slightly slower for the D atom reaction compared to that for the H atom reaction. As shown by the present temperature-dependent measurements, the activation energy for H abstraction by D seems to be somewhat higher than for the analogous abstraction reaction by the H atoms. This may hint at a contribution to the reaction from tunneling through the potential energy barrier, which would be favored for the H atom reaction.

The observed two product channels can be rationalized by the scheme

$$D + H_2CO \xrightarrow{a} HD + HCO \qquad (2a)$$

$$D + H_2CO \underset{-b}{\overset{b}{\rightleftharpoons}} CH_2DO^* \xrightarrow{c} H + HDCO \qquad (2b,-2b,2c)$$

$$\xrightarrow{d} HD + HCO \qquad (2d)$$

$$\xrightarrow{e} H_2 + DCO \qquad (2e)$$

$$\xrightarrow[+M]{f} CH_2DO \qquad (2f)$$

$$D + H_2CO \underset{-g}{\overset{g}{\rightleftharpoons}} CH_2OD^* \xrightarrow{h} H + HDCO \qquad (2g,-2g,2h)$$

$$\xrightarrow[+M]{i} CH_2OD \qquad (2i)$$

Not all of these channels are expected to play a role. As mentioned, the collisional stabilization channels (2f and 2i) require high pressure. Furthermore, the energy barrier for the dissociation of the CH_2DO^* complex to HD + HCO (2d) or H_2 + DCO (2e) is assumed to be significantly higher than that for the dissociation of the complex to $D + H_2CO$ (−2b) or H + HDCO (2c).[22] According to ab initio calculations,[23−27] the addition of D to the O atom of the H_2CO molecule (2g) has a significantly higher energy barrier than the addition to the C atom. Reaction 2h requires an isomerization according to $CH_2OD \rightleftarrows CHDOH$ or $CH_2OD \rightleftarrows CH_2DO$, again with high energy barriers.

Thus, the reactions which have to be considered are 2a, 2b, −2b, and 2c. In this sequence, reaction 2c is favored compared to −2b because of the difference in the zero-point energy[28] between H_2CO and HDCO ($\Delta E_Z = -590\ cm^{-1}$).

With these premises and with the usual steady-state assumption for CH_2DO^*, the experimental rate constant $k_{2.2}$ for the D/H isotope exchange is found to be

$$k_{2.2} = k_{2b}k_{2c}/(k_{-2b} + k_{2c})$$

Thus, the experimental results for $k_{2.2}$ can be used to determine the value of the $D + H_2CO$ association rate constant k_{2b}, which should give the rate constant for the formation of the addition product CH_2DO in the high-pressure limit. The molecular parameters of these calculations are listed in Table 5. The ratio $k_{2c}/(k_{-2b} + k_{2c})$ was estimated from the specific rate constants $k(E,J)$ of the respective CH_2DO^* dissociation channels at energy E and angular momentum J using unimolecular rate theory.[30] Because $k_{2c} > k_{-2b}$, the correction to the experimental $k_{2.2}$ was expected to be rather small. Thus, $k_{2c}/(k_{-2b} + k_{2c})$ was calculated for simplicity by adopting average values for E and J of the intermediate CH_2DO^* complex from step 2b, giving $k_{2c}/(k_{-2b} + k_{2c}) = 0.83$ and 0.8 at 296 and 600 K, respectively. With the correction, the expression of the rate constant for the $D + H_2CO$ association reaction as a function of temperature becomes

$$k_{2b}(T) = (7.8 \pm 2.0) \times 10^{12} \times \exp[-(14.9 \pm 0.8)\ kJ\ mol^{-1}/RT]\ cm^3\ mol^{-1}\ s^{-1}$$

This experimental rate expression can be compared with predictions on the basis of the unimolecular rate theory. Using the standard transition-state theory expression for the high-pressure thermal association rate constant,[30] the pre-exponential factors were calculated as $A = 9.2 \times 10^{12}\ cm^3\ mol^{-1}\ s^{-1}$ (T = 296 K) and $1.1 \times 10^{13}\ cm^3\ mol^{-1}\ s^{-1}$ (T = 600 K), almost independent of T in the range of interest. The resulting small curvature in the corresponding Arrhenius plot from the small temperature dependence of the A value would be described by a $T^{0.22}$ term. This calculated A factor is slightly larger than the

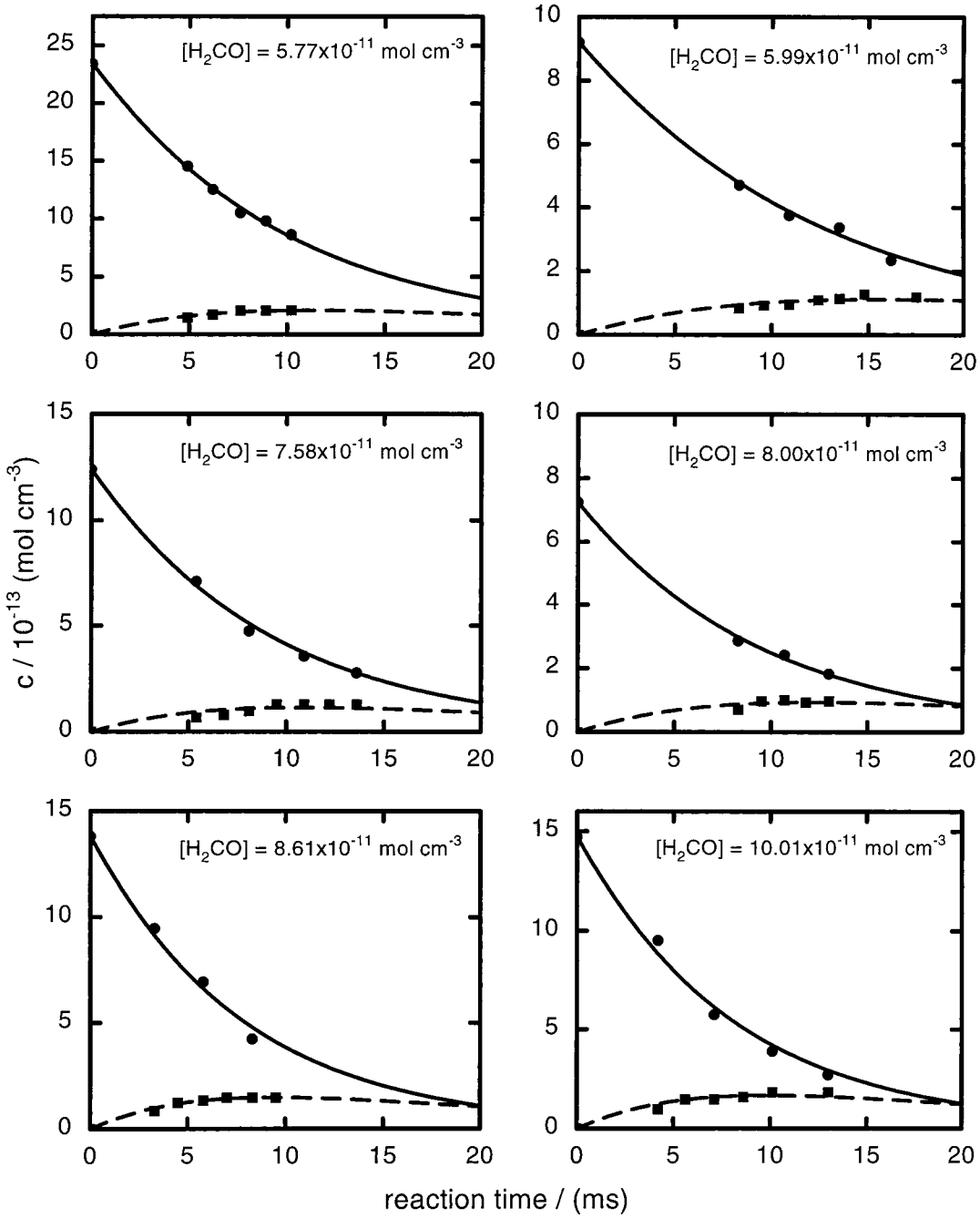

Figure 5. Measured concentration−time profiles of the D and H atoms in the reaction system D + H_2CO at $T = 600$ K. Experimental concentrations: ● = D, ■ = H. Simulated concentration profiles: —. The rate constant values $k_{2.1}$ and $k_{2.2}$ from the fitting are given in Table 4.

experimental one. However, the rate constants are expected to be affected by tunneling. Tunneling has been shown to be important from the measurements of the state-specific CH_3O unimolecular decay rate constants we reported earlier.[31] The respective contributions for the D + H_2CO addition step could be estimated for the purpose of the present study as proposed by Troe[32] by assuming a simple parabolic potential barrier shape. The calculated tunneling factors were $F_{tunnel} = 1.48$ at $T = 296$ K and $F_{tunnel} = 1.17$ at $T = 600$ K. With this correction, the expression for k_{2b} without tunneling contribution derived from the experimental data is $k_{2b}(T) = (8.2 \pm 2.0) \times 10^{12} \exp[-(16.0 \pm 0.8)\ \text{kJ mol}^{-1}/RT]\ \text{cm}^3\ \text{mol}^{-1}\ \text{s}^{-1}$. Within the experimental error, this A factor is in very good agreement with the result from the transition-state theory calculation above.

When the theoretical value of $A = 9.2 \times 10^{12}\ \text{cm}^3\ \text{mol}^{-1}\ \text{s}^{-1}$ is combined with the room-temperature experimental result for k_{2b}, the classical potential barrier height ΔE_0 of the D + H_2CO addition reaction should be

$$\Delta E_0(\text{D} + \text{H}_2\text{CO}) = 1360 \pm 100\ \text{cm}^{-1}$$

With the change in zero-point energy at the transition-state configuration, the resulting value for the H + H_2CO addition reaction would be

$$\Delta E_0(\text{H} + \text{H}_2\text{CO}) = 1540 \pm 150\ \text{cm}^{-1}$$

Both values are considered as upper limits because of the higher theoretical A factor used for their estimation. The lower experimental A factor of $8.2 \times 10^{12}\ \text{cm}^3\ \text{mol}^{-1}\ \text{s}^{-1}$ would give barriers lower by 20 cm^{-1}. This uncertainty is small, however,

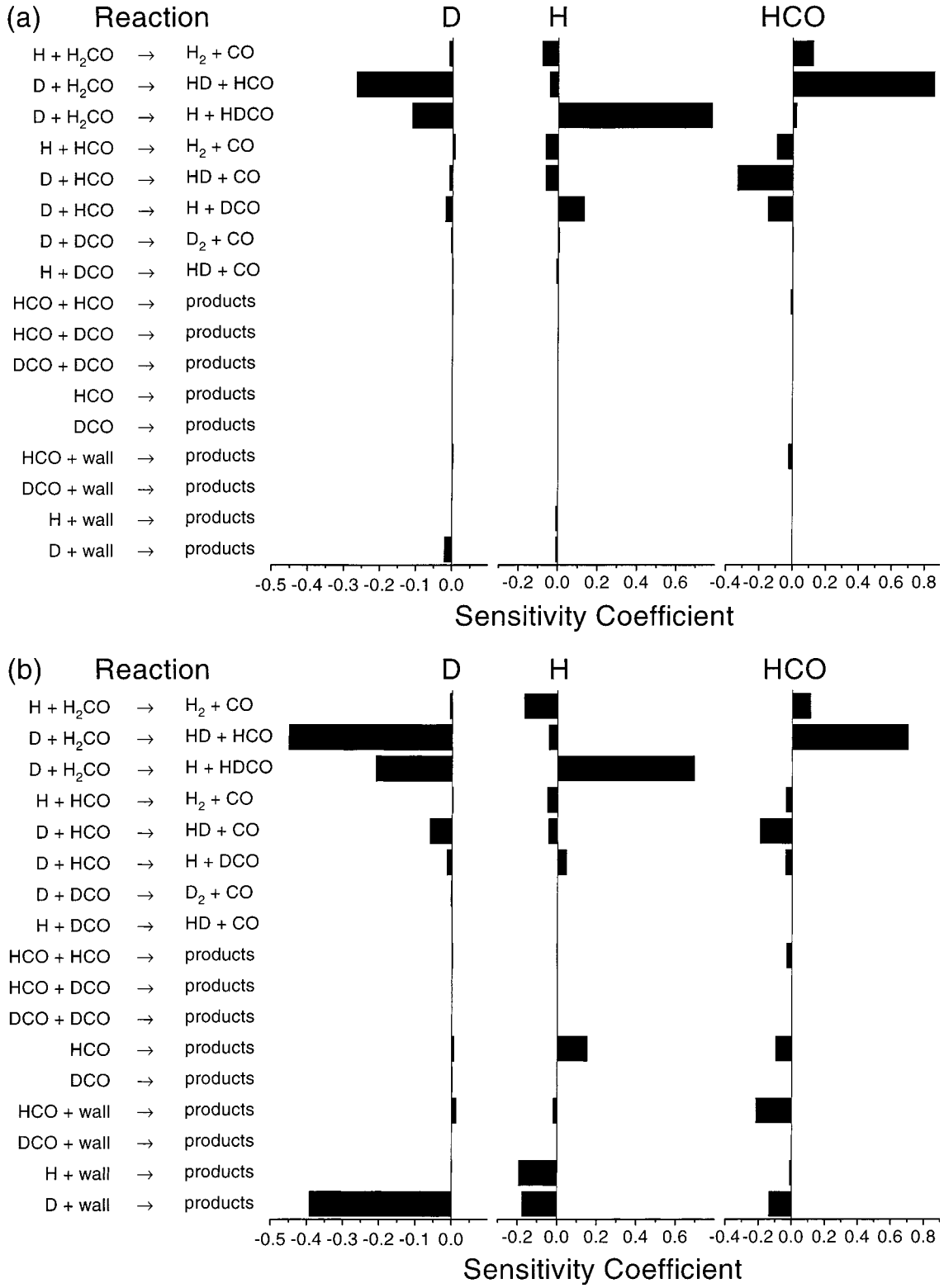

Figure 6. Results of the sensitivity analysis for the reaction system D + H_2CO at (a) $T = 296$ K, $[D]_0 = 1.29 \times 10^{-12}$ mol cm^{-3}, $[H_2CO]_0 = 6.91 \times 10^{-10}$ mol cm^{-3}, and $t = 10$ ms and at (b) $T = 600$ K, $[D]_0 = 1.24 \times 10^{-12}$ mol cm^{-3}, $[H_2CO]_0 = 7.58 \times 10^{-11}$ mol cm^{-3}, and $t = 10$ ms.

considering the larger uncertainty of the zero-point energy correction between the D and the H atom reactions because of the high-frequency vibrations of the D−$H_2CO^{‡}$ transition state, which had to be estimated.

The estimates for the classical barrier heights based on the present experimental rate constants can be compared with data from several ab initio studies,[23−27] which gave results in the range 1600 cm^{-1} ≤ ΔE_0(H + H_2CO) ≤ 4300 cm^{-1}. Clearly the theoretical values are, in general, on the high side.

These results also have considerable bearing for the unimolecular dissociation of the CH_3O radical. The heat of formation[33] of CH_3O and the classical potential barrier height for the reaction $CH_3O \rightarrow H + H_2CO$ have long been controversial. Under the experimental conditions used to measure the thermal rate constants,[34−37] the CH_3O dissociation reaction is in the low-pressure regime so that significant corrections have to be applied to determine the dissociation threshold energy. The resulting ΔE_0 values for $CH_3O \rightarrow H + H_2CO$ are in the range 8300 cm^{-1}

$\leq \Delta E_0 \leq 8500$ cm^{-1}. Direct vibration−rotation quantum-state-resolved measurements of the CH_3O dissociation in our laboratory[31] gave $\Delta E_0 = 8400$ cm^{-1}.

Recent photodetachment studies of CH_3O^- have produced a consensus value for the heat of formation of CH_3O of $\Delta_f H_0^0(CH_3O) = 28.5$ kJ mol^{-1}.[38,39] Taking the dissociation energy $\Delta_r H_0^0(CH_3O \rightarrow H + H_2CO) = 6920$ cm^{-1} derived from that value and from $\Delta E_0(H + H_2CO \rightarrow CH_3O) = 1540$ cm^{-1}, the classical threshold energy for the CH_3O unimolecular dissociation should be $\Delta E_0(CH_3O \rightarrow H + H_2CO) = 8460 \pm 200$ cm^{-1}, in good agreement with the experimental data.[32]

5. Conclusions

(1) The reaction between D atoms and H_2CO proceeds via two different reaction channels. The first pathway is the direct abstraction of one of the H atoms. The second channel proceeds via an addition of the D atom to the carbon atom of the aldehydic CO group, resulting in an intermediate vibrationally highly excited CH_2DO^* adduct.

(2) The classical potential energy barrier height, including zero-point energies for the addition of D to the C atom of the CO group, is $\Delta E_0(D + H_2CO) = (1360 \pm 100)$ cm^{-1}.

(3) At low pressure, the addition step is followed by an elimination of an H atom or a D atom. The H elimination results in a D/H isotope exchange, which has been observed, whereas the D elimination is equivalent with a redissociation to the reactants. The branching between the H or D atom elimination is determined by the ratio of the specific rate coefficients $k(E,J)$ of the CH_2DO^* adduct for the two pathways. The H atom elimination is favored by the difference in the zero-point energy between H_2CO and HDCO, $\Delta E_Z = -590$ cm^{-1}.

(4) At high pressure, the vibrationally highly excited CH_2DO^* adduct will be collisionally stabilized to the product CH_2DO. The falloff curve may be evaluated using unimolecular rate theory.[30]

(5) An addition of a D atom to the O atom of the CO aldehydic group has been calculated to have a much higher potential energy barrier.[23−27] This reaction is ruled out as a simple explanation for the observed D/H isotope exchange process because of the high energies of HCOH/HCOD.

(6) At room temperature and low pressure, the measured branching ratio between the H abstraction and the D/H elimination channels of the $D + H_2CO$ reaction is $k_{2.1}/k_{2.2} = 1.27$.

(7) The reaction between H atoms and H_2CO normally proceeds via direct H atom abstraction. At high pressures, the addition of an H atom to the C atom of the aldehydic CO group leads to CH_3O as an additional reaction product.

(8) The classical potential-energy barrier height, including zero-point energies for the H atom addition to the C atom of the CO group, is $\Delta E_0(H + H_2CO) = 1540 \pm 150$ cm^{-1}. Because of the higher barrier, the H atom abstraction channel dominates the $H + H_2CO$ reaction. The addition of an H atom to the O atom of the CO aldehydic group is unlikely to be of importance.

(9) The threshold energy (including zero-point energies) for the unimolecular dissociation of CH_3O should be $\Delta E_0(CH_3O \rightarrow H + H_2CO) = 8460 \pm 200$ cm^{-1}, in agreement with recent experimental data.[32]

(10) Analogous H atom addition channels may also be expected for reactions of H atoms with larger aldehydes and ketones, where a collisional stabilization of the adducts may occur at lower pressures. Corresponding evidence has been reported, for example, for the reaction of H atoms with CH_3CHO.[40] Further experimental studies of these reactions are desired.

Acknowledgment. The authors acknowledge financial support of this work by the Deutsche Forschungsgemeinschaft and the Fonds der Chemischen Industrie and by a grant from the Hungarian-German Intergovernmental Science and Technology Cooperation Programme.

References and Notes

(1) Okabe, H. *Photochemistry of Small Molecules*; Wiley: New York, 1978.

(2) Atkinson, R.; Baulch, D. L.; Cox, R. A.; Hampson, R. F.; Kerr, J. A.; Troe, J. *J. Phys. Chem. Ref. Data* **1992**, *21*, 1125.

(3) Moore, C. B.; Weisshaar, J. C. *Annu. Rev. Phys. Chem.* **1983**, *34*, 525.

(4) Mallard, W. G.; Westley, F.; Herron, J. T.; Hampson, R. F.; Frizelli, D. H. *NIST Chemical Kinetics Database, Version 2Q98*; NIST Standard Reference Database 17: Gaithersburg, MD, 1998.

(5) Atkinson, R.; Baulch, D. L.; Cox, R. A.; Hampson, R. F.; Kerr, J. A.; Rossi, M. J.; Troe, J. *Summary of IUPAC Evaluated Kinetic and Photochemical Data for Atmospheric Chemistry*; IUPAC Subcommittee on Gas Kinetic Data Evaluation for Atmospheric Chemistry. (http://www.iupac-kinetic.ch.cam.ac.uk, accessed in 2000).

(6) Chang, J. S.; Barker, J. R. *J. Phys. Chem.* **1979**, *83*, 3059.

(7) Ferrieri, R. A.; Wolf, A. P. *J. Phys. Chem.* **1992**, *96*, 7164.

(8) Dupuis, M.; Lester, W. A. *J. Chem. Phys.* **1984**, *80*, 4193. Dupuis M.; Lester, W. A. *J. Chem. Phys.* **1984**, *81*, 847. Neely, W. C.; Newhouse, E. I.; Pathirana, S.; Worley, S. D. *Chem. Phys. Lett.* **1989**, *155*, 381.

(9) Tanzawa, T.; Klemm, R. B. *American Chemical Society National Meeting*; American Chemical Society: Washington, DC, 1979.

(10) Wellman, J.; Park, J.; Hershberger, J. F. *Chem. Phys. Lett.* **1991**, *178*, 405.

(11) Su, F.; Calvert, J. G.; Shaw, J. H. *J. Phys. Chem.* **1979**, *83*, 3185. Barnes, I.; Becker, K. H.; Fink, E. H.; Reimer, A.; Zabel, F.; Niki, H. *Chem. Phys. Lett.* **1985**, *115*, 1. Jemi-Alade, A. A.; Lightfoot, P. D.; Lesclaux, R. *Chem. Phys. Lett.* **1992**, *195*, 25.

(12) Dóbé, S.; Oehlers, C.; Temps, F.; Wagner, H. Gg.; Ziemer, H. *Ber. Bunsen-Ges. Phys. Chem.* **1994**, *98*, 754.

(13) Ziemer, H. Ph.D. Thesis, University of Göttingen, Göttingen, Germany, 1994.

(14) Westenberg, A. A. *Prog. React. Kinet.* **1973**, *7*, 23.

(15) Sappey, A. D.; Crosley, D. R. *J. Chem. Phys.* **1990**, *93*, 7601. Meier, U. E.; Hunziker, L. E.; Crosley, D. R. *J. Phys. Chem.* **1991**, *95*, 5163.

(16) Ziemer, H.; Dóbé, S.; Wagner, H. Gg.; Olzmann, M.; Viskolcz, B.; Temps, F. *Ber. Bunsen-Ges. Phys. Chem.* **1998**, *102*, 897.

(17) Temps, F.; Wagner, H. Gg. *Ber. Bunsen-Ges. Phys. Chem.* **1984**, *88*, 410.

(18) Timonen, R. S.; Ratajczak, E.; Gutman, D.; Wagner, A. F. *J. Phys. Chem.* **1987**, *91*, 5325.

(19) Gear, C. W. *Numerical Initial Value Problems in Ordinary Differential Equations*; Prentice Hall: Englewood Cliffs, 1971. Gear, C. W. *Commun. ACM* **1971**, *14*, 176.

(20) Bevington, P. R. *Data Reduction and Error Analysis for the Physical Sciences*; McGraw-Hill: New York, 1969.

(21) Irdam, E. A.; Kiefer, J. H.; Harding, L. B.; Wagner, A. F. *Int. J. Chem. Kinet.* **1993**, *25*, 285.

(22) Seakins, P. W.; Leone, S. R. *J. Phys. Chem.* **1992**, *96*, 4478.

(23) Sæbø, S.; Radom, L.; Schaefer H. F. *J. Chem. Phys.* **1983**, *78*, 845.

(24) Melius, C. F. *Heats of Formation and Free Energies*; Sandia National Laboratories: Livermore, CA, 1990.

(25) Page, M. *Eastern States Meeting*; Combustion Institute: Albany, NY, 1989.

(26) Sosa, C.; Schlegel, H. B. *Int. J. Quantum Chem.* **1986**, *29*, 1001.

(27) Walch, S. P. *J. Chem. Phys.* **1993**, *98*, 3076.

(28) Herzberg, G. *Molecular Spectra and Molecular Structure*; Van Nostrand Reinhold: New York, 1966; Vol. 3. Reisner, D. E.; Field, R. W.; Kinsey, J. L.; Dai, H.-L. *J. Chem. Phys.* **1984**, *80*, 5968. Job, V. A.; Sethuraman, V.; Innes, K. K. *J. Mol. Spectrosc.* **1969**, *30*, 365.

(29) Temps, F. Technical Report 11/95; MPI für Strömungsforschung: Göttingen, Germany, 1995.

(30) Troe, J.; Wagner, H. Gg. *Ber. Bunsen-Ges. Phys. Chem.* **1967**, *71*, 1967. Troe, J. *J. Phys. Chem.* **1979**, *83*, 114.

(31) Dertinger, S.; Geers, A.; Kappert, J.; Wiebrecht, J.; Temps, F. *Faraday Discuss.* **1995**, *102*, 31.

(32) Troe, J. Tunneling. In *The Jerusalem Symposia on Quantum Chemistry and Biochemistry*; Jortner, J., Pullman, B., Eds.; Reidel: Dordrecht, The Netherlands, 1986.

(33) Berkowitz, J.; Ellison, G. B.; Gutman, D. *J. Phys. Chem.* **1994**, *98*, 2744.

(34) Batt, L. *Int. J. Chem. Kinet.* **1979**, *11*, 977; *Int. Rev. Phys. Chem.* **1986**, *6*, 53.

(35) Page, M.; Lin, M. C.; He, Y.; Choudhoury, T. K. *J. Phys. Chem.* **1989**, *93*, 4404. Choudhoury, T. K.; He, Y.; Sanders, W. A.; Lin, M. C. *J. Phys. Chem.* **1990**, *94*, 2394.

(36) Wantuck, P. J.; Oldenborg, R. C.; Baughcum, S. L.; Winn, K. R. *Twenty-Second Symposium (International) On Combustion*; Combustion Institute: Pittsburgh, PA, 1988; p 973.

(37) Oguchi, T.; Miyoshi, A.; Koshi, M.; Matsui, H. *Bull. Chem. Soc. Jpn.*, **2000**, *73*, 53.

(38) Osborn, D. L.; Leahy, D. J.; Ross, E. M.; Neumark, D. M. *Chem. Phys. Lett.* **1995**, *235* 484.

(39) Ramond, T. M.; Davico, G. E.; Schwartz, R. L.; Lineberger, W. C. *J. Chem. Phys.* **2000**, *112*, 1158.

(40) Becerra, R.; Frey, H. M. Unpublished results.